

# Crack widths in reinforced cement-based structures

A.P. Fantilli, P. Vallini

*Politecnico di Torino, Torino, Italy*

H. Mihashi

*Tohoku University, Sendai, Japan*

**ABSTRACT:** The theoretical approaches used for the evaluation of crack width in reinforced concrete (RC) structures, are generally based on the hypothesis of parallel crack surfaces. In this way, crack width measured on the concrete cover should be equal to that on the bar surface. The results of several experimental analyses do not justify this assumption. Therefore, to better define the effective crack profile of RC structures, a new model, able to analyze the whole structural response of reinforced concrete ties, is here presented. In the proposed approach, all the physical phenomena involved in the cracking process are taken into account. A good agreement between numerical results and experimental data is found both in case of steel rebar and ordinary Fiber Reinforced Cementitious Composites (R/FRCC), and in case of steel rebar and High Performance Fiber Reinforced Cementitious Composites (R/HPFRCC).

## 1 INTRODUCTION

The demand of improving and increasing durability of reinforced concrete (RC) structures, which are generally deteriorated by the corrosion of steel reinforcement, has driven several researchers to analyzing the cracking phenomenon of concrete in tension. As a first approach, crack pattern evolution has been experimentally investigated in RC members in tension since the second half of the past Century (Broms, 1965; Goto, 1971; Watstein & Mathey, 1959). Such elements are generally composed of a steel reinforcing bars ( $\Phi$  is the diameter of its cross-section) covered by a concrete cylinder of thickness  $R_1 - \Phi/2$  (Fig. 1a). During the test, when the normal load  $N$  is applied to the ends of the element, a crack pattern composed by different types of cracks appears. Precisely, the cracking process produces both main cracks, which are observed on the surface of the tie, and internal (or hidden) cracks (Fig. 1b), which are not visible to an external viewer. They have been detected in the experimental analyses of Broms (1965) and Goto (1971) by injecting ink into the specimen during the loading. After the ink had hardened, the tested member was cut open and the internal cracks were measured both in width and in length.

The cracking phenomenon mainly affects RC structures subjected to bending actions. Anyway, it is a widespread opinion that a RC tie is a satisfactory model for reproducing the tensile regions between two consecutive cracks of a flexural member. In

other words, modeling RC members in tension can be considered a reasonable way to compute all the phenomena involved in the cracking of RC structures. Therefore, the first theoretical researches on the evolution of main cracks have regarded RC ties. In these elements, according to the linear elastic fracture mechanics theory, the growth of a single crack can be analyzed as a stability problem (Bianchini et al., 1968). For instance, it is possible to investigate the evolution of a crack profile, or the function  $w(R)$  (that is, the crack width  $w$  measured at the distance  $R$  from the reinforcement axis), in the portion depicted in Figure 1b. If a crack is supposed to start from the steel - concrete interface (where  $R = \Phi/2$ ), its propagation is initially stable, and it does not reach the surface of the member (where  $R = R_1$ ). This is the condition of internal cracks in Figure 1b, for which the stress intensity factor  $K_I$  is lower than the critical value  $K_{IC}$ . By increasing of the normal force  $N$ ,  $K_I$  becomes higher than  $K_{IC}$ , and crack propagation is unstable. In this case, crack tip rapidly reaches the external surface (main cracks in Fig. 1b). As is well known, the value of  $K_I$  is strictly connected to the geometry of the problem and to the mechanical properties of concrete.

Therefore, in the case of Figure 1b, only when the distance  $l_c$  between main cracks is much longer than the thickness of the concrete cover ( $l_c \gg R_1 - \Phi/2$ ), can the crack tip rise to concrete surface. On the contrary, if  $l_c < (R_1 - \Phi/2)$ , the propagation of internal cracks remains stable, and their tips do not reach the external surface.

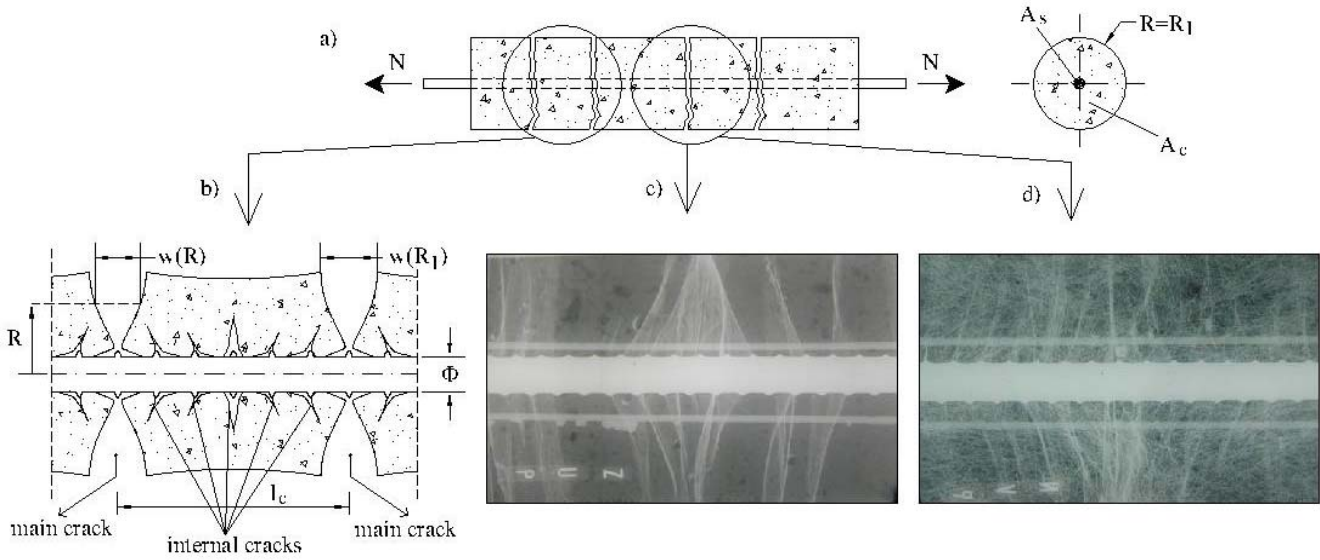


Figure 1: Main cracks and internal cracks in reinforced concrete structures: a) steel reinforced members subjected to axial loads; b) a portion of a RC tie (Goto, 1971); c) a portion of a R/FRCC tie; d) a portion of a R/HPFRCC tie (Mihashi et al. 2003).

Therefore, main cracks can be considered as the final stage of the unstable propagation of internal cracks, which are initially stable. This assumption is in accordance to the tests of Broms (1965) and Goto (1971), and to the numerical investigations of Lutz (1970), which confirmed the presence of main cracks and internal cracks at all the loading stages.

Starting from these theoretical and experimental observations, many formulae for the evaluation of crack width, and crack distance, have been proposed (ACI Committee 224, 1986; CEB, 1993). However, as recently pointed out by Beeby (2004), in these approaches crack width on the surface of the concrete cover,  $w(R_1)$ , is assumed to be equal to that on the steel-concrete interface,  $w(\Phi/2) = w_0$ . This assumption disagrees with the results of several tests, where crack shapes [i.e. the crack profile  $w(R)$ ] have been measured. Such investigations have been initially conducted by Broms (1965), who has observed and measured the evolution of main cracks (Fig. 1b). At low axial loads  $N$ , crack widths are nearly the same, independently of the distance  $R$  from the reinforcement [ $w(R) \cong \text{constant}$  in Fig. 1b]. In this situation, crack surfaces are approximately plane and perpendicular to the reinforcement axis. Subsequently, with the increase of  $N$ , crack widths are narrower on the reinforcement, where  $w_0$  becomes approximately 1/2 to 1/3 of  $w(R_1)$ . Similar conclusions have been drawn by Beeby (1972), who has tested several tension members with different dimensions and reinforcement ratios.

The distribution of tensile stresses  $\sigma_{ct}$  in the concrete cover is the fundamental cause of different crack widths along a main crack. Since  $\sigma_{ct}(R) \neq \text{constant}$  on crack surfaces, shear stresses, originated by the bond-slip between steel and concrete, can be detected in the concrete surrounding the main cracks. According to Watstein & Mathey (1959), the shear components of stress give rise to

the crack profile  $w(R)$  shown in Figure 1b. Thus, it is not sufficient to take into account only the bond-slip mechanism between steel and concrete and the fracture mechanics of concrete, as proposed by Fantilli et al. (1998). To evaluate the crack profile of a main crack, the shear deformability of concrete cannot be neglected (Walraven & Reinhardt, 1981).

In order to take into account all the mechanisms involved in the cracking phenomenon, a new model, able to compute the structural response of a member in tension, is presented in this paper. Not only the tensile members made of classical concrete, but also those made by ordinary Fiber Reinforced Cementitious Composite (FRCC) and by High Performance Fiber Reinforced Cementitious Composite (HPFRCC) are taken into consideration. In these new cement-based composites, crack profiles appear different from those depicted in Figure 1b. As observed in the tests by Mihashi et al. (2003) and Otsuka et al. (2003), even for high steel strains, crack widths away from the bars, of reinforced FRCC (R/FRCC) and reinforced HPFRCC (R/HPFRCC) members in tension, are narrower than those directly measured over the reinforcement surface. This is shown by the two X-ray images reported in Figures 1c-1d, which have been taken at yielding of steel rebar in tensile members made, respectively, of R/FRCC (Fig. 1c) and of R/HPFRCC (Fig. 1d).

## 2 A MODEL FOR THE EVALUATION OF CRACK PROFILE

The evaluation of crack profiles of a main crack cannot be separated from the structural analysis of the tension member depicted in Figure 1a.

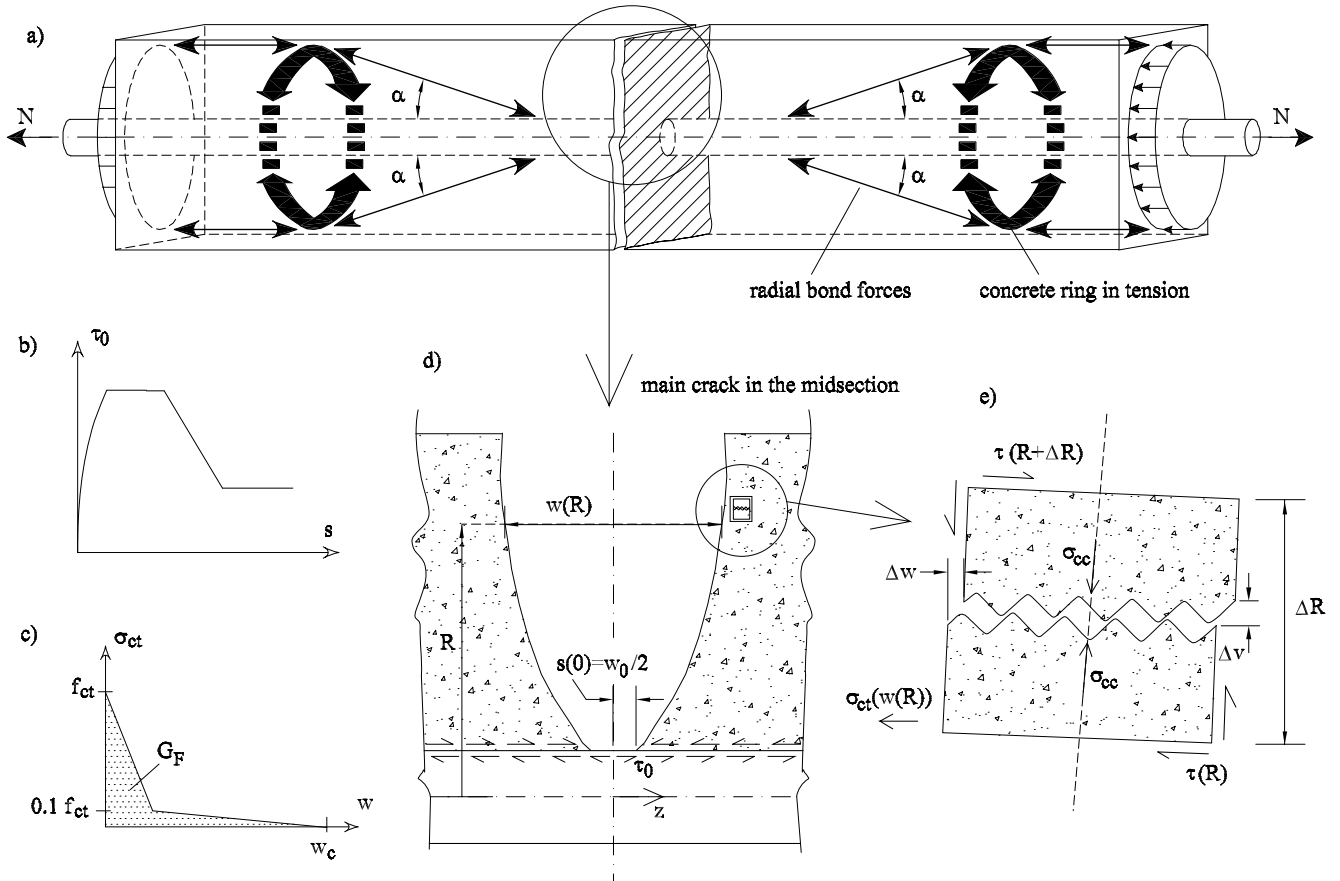


Figure 2: First crack in the midsection of a RC tie: a) the strut and tie model of Tepfers (1979); b) bond-slip  $\tau_0-s$  relationship (CEB, 1993); c) fictitious crack model  $\sigma_{ct}-w$  (CEB, 1993); d) crack profile of the main crack in the midsection of the element; e) kinematic and static variables of the Rough Cracks model (Bazant & Gambarova, 1980).

The mechanical response of RC ties can be computed by referring to the well-known strut and tie model introduced by Tepfers (1979), which is schematically shown in Figure 2a. It consists of radial components of the bond forces, inclined of  $\alpha$  with respect to reinforcement axis and produced by the ribs of the rebar, which are balanced against tensile stress rings. Such a mechanism correctly reproduces an anchorage zone, but it vanishes in the midsection of the RC member in tension depicted in Figure 1a. In this zone, concrete is less confined than elsewhere (Fig. 2a), due to the absence of a tensile stress ring near the external surface. Thus, the first main crack usually develops in the middle of the element.

For the sake of simplicity, the definition of crack profiles  $w(R)$  will regard a RC tie with a single main crack in its midsection. The effects produced by other cracks, such as the internal cracks (Fig. 1b), are indirectly considered by adopting the phenomenological relationships  $\tau_0-s$  depicted in Figure 2b, which reproduces the bond-slip behavior between steel and concrete. Since this mechanism generates bond stresses  $\tau_0$  around the concrete-rebar interface of the cracked cross-section, shear stresses can be detected in the surrounding concrete. According to several experimental and theoretical observations, shear stresses (and shear strains) produce different crack widths along  $R$ . In particular, crack width  $w_0$  on the bar surface, whose magnitude is related to the

bond stress by the  $\tau_0-s$  relationship of Figure 2b (in which  $s = w_0/2$  has to be considered), is different from  $w(R)$  measured at distance  $\Phi/2 < R \leq R_1$  (Fig. 2d). However, not only shear stresses  $\tau$  affect the concrete around the cracks. In an element closer to the crack surfaces (Fig. 2e), the axial tensile stresses  $\sigma_{ct}$  and radial compressive stresses  $\sigma_{cc}$ , produced by the bond mechanism in the Tepfers' model, can be also detected. According to the Fictitious Crack model introduced by Hillerborg et al. (1976),  $\sigma_{ct}$  is a function of the crack width  $w(R)$ , as shown by the cohesive relationship of Figure 2c. The single discrete crack can be divided into two different zones: the process zone, where  $w(R) \leq w_c$  (and  $\sigma_{ct} \geq 0$ ), and the macro-cracked zone, where  $w(R) > w_c$  (and  $\sigma_{ct} = 0$ ). Shear stresses  $\tau$  and compressive stresses  $\sigma_{cc}$  are governed by the so-called aggregate interlock mechanism. It has been investigated for a long time, and different models have been proposed to reproduce it theoretically (Bazant & Gambarova, 1980). An aggregate interlock model is generally found on the definition of the relationship between the kinematical variables (i.e., the increment of the longitudinal displacement, or crack width,  $\Delta w$ , and the increment of the radial displacement  $\Delta v$ ) and static variables (i.e., shear stresses  $\tau$  and compressive stresses  $\sigma_{cc}$ ). The Rough Cracks model introduced by Bazant & Gambarova (1980) is here adopted for the aggregate interlock mechanism. It has been

widely used to reproduce effectively the shear resistance of RC beams (Dei Poli et al., 1986). In particular, in the present paper, the Rough Cracks model is considered in the form of shear stress increment  $\Delta\tau$  within the element of finite length  $\Delta R$  (Fig. 2e) (Gambarova, 1980):

$$\Delta\tau = \tau(R + \Delta R) - \tau(R) = \tau_a \cdot \frac{a_0}{a_0 + (\Delta v/d_a)^2} \cdot \frac{\Delta w}{\Delta v} \cdot \frac{a_2 + a_3|\Delta w/\Delta v|^3}{1 + a_3(\Delta w/\Delta v)^4} \quad (1)$$

where  $\tau_a = 0.25 f_c$  ( $f_c$  = compressive strength of concrete);  $a_0 = 0.111$ ;  $a_1 = 0.435E-3$  N/mm;  $a_2 = 2.45/\tau_a$  MPa;  $a_3 = 2.44 (1-4/\tau_0)$  MPa;  $d_a$  = maximum aggregate size. If the function of radial displacement increment  $\Delta v$  and the function of shear stress  $\tau(R)$  are known, the increment of the crack profile  $\Delta w(R)$  can be obtained by solving Eq. (1).

## 2.1 The shear stress function $\tau(R)$

The shear stress function  $\tau(R)$  can be defined by imposing the equilibrium condition in the longitudinal direction. More precisely, referring to the concrete cylinder of length  $dz$  depicted in Figure 3, whose cross-section is a circular crown defined by the radius  $R_0$  and  $R$ , it is possible to write:

$$-2\pi R \tau(R) dz + 2\pi R_0 \tau(R_0) dz + \int_{R_0}^R \frac{\partial \sigma_{ct}}{\partial z} dz dA_c = 0 \quad (2)$$

where  $\tau(R)$  = shear stress on the external surface of the cylinder;  $\tau(R_0)$  = shear stress on the internal surface and of the cylinder;  $\sigma_{ct}$  = longitudinal tensile stress in the concrete (due to symmetry the radial stresses are assumed to be equal to zero).

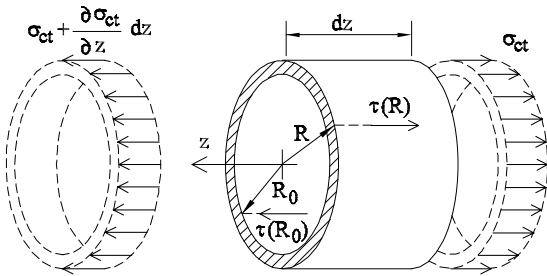


Figure 3: The state of stress in a concrete cylinder of length  $dz$ . Neglecting small quantities of higher order, the cross-sectional area  $dA_c$  can be evaluated with the following formula:

$$dA_c = 2\pi R dR \quad (3)$$

By assuming  $R_0 = \Phi/2$ , the function  $\tau(R)$  can be found by substituting Eq. (3) into Eq. (2):

$$\tau(R) = \frac{\tau_0 \cdot \Phi}{2 \cdot R} [1 + \gamma(R)] \quad (4)$$

where  $\tau_0$  = bond stress on the bar surface, whose magnitude depends on the crack width  $w_0$  (according to the  $\tau_0$ - $s$  relationship of Fig. 2b). The function  $\gamma$  may be written as:

$$\gamma(R) = \frac{2}{\tau_0 \Phi} \int_{R_0}^R \frac{\partial \sigma_{ct}}{\partial z} R dR \quad (5)$$

To evaluate  $\gamma(R)$ , the function  $\partial \sigma_{ct}/\partial z$  should be defined. It is important to clarify that the crack of Figure 2d, as well as those considered in this paper, are located in the symmetrical cross-section of a tensile element. Thus, shear stresses  $\tau$  are not admitted on crack surfaces, while possible interactions between the Fictitious Crack Model of Figure 2c and the Rough Crack model of Figure 2e are completely neglected. Shear stresses, originated by the bond-slip mechanism on the bar surface, are only transmitted to the upper layers by shear transfer mechanism.

This mechanical behavior is schematically reproduced in Figure 4a. In this way, the shape of crack profile suggests the shape of  $\tau(R)$ . For instance, it is possible to analyze the crack profile shown in Figure 4a, where the distances of the concrete surface and crack tip from the reinforcement axis are, respectively,  $R_1$  and  $R_B$ . From the concavity of  $w(R)$ , the sign (i.e. the direction) of shear stresses in each point of the crack surface can be immediately defined. It can be concordant or discordant to the direction of  $\tau_0$ , which is produced by the bond slip mechanism on steel surface. Obviously,  $\tau=0$  in the point of the profile where  $w=0$ , and in the point where the derivative  $dw/dR$  changes its sign (the radius  $R_A$  is assumed to be the distance between this point and the reinforcement axis). In this way, a qualitative shape of  $\tau(R)$  is therefore obtained (Fig. 4a).

According to the tests of Broms (1956) and Goto (1971), and to the theoretical results of Bianchini et al. (1968), all the possible crack profiles are shown in Figures 4b-4d. For low values of  $N$ , crack is extended within the concrete thickness (internal crack) and it does not appear on the concrete surface (Fig. 4a). Increasing  $N$ , crack grows (Fig. 4b) and its tip reaches and overcomes the external surface ( $R_B = R_1$  in Fig. 4c). If  $N$  remains low,  $w(R) \cong \text{constant}$  and crack surfaces can be considered plane and vertical. On the contrary, for higher values of the applied loads, crack width is shorter on the reinforcement than on the concrete surface (Fig. 4d).

In Figure 4, shear stress distributions  $\tau(R)$ , corresponding to the crack profiles of a main crack, are also depicted. In the cases of Figures 4b-4c, when  $R_A < R_1$ , the values of shear stresses are zero in two different points, which are located at two different depths from the reinforcement axis ( $R_A$  and  $R_B$ ).

More exactly, in the zone where  $R_A < R < R_B$ , shear stresses are discordant to the direction of bond stress  $\tau_0$ . When  $R_A = R_B$  (Fig. 4d),  $\tau(R)$  is monotonic and shear stresses have the same sign of  $\tau_0$  for all the values of  $R$ . In this situation,  $\tau(R)$  seems to be independent of crack width and, consequently, of the cohesive law  $\sigma_{ct} - w$  (Fig. 2c).

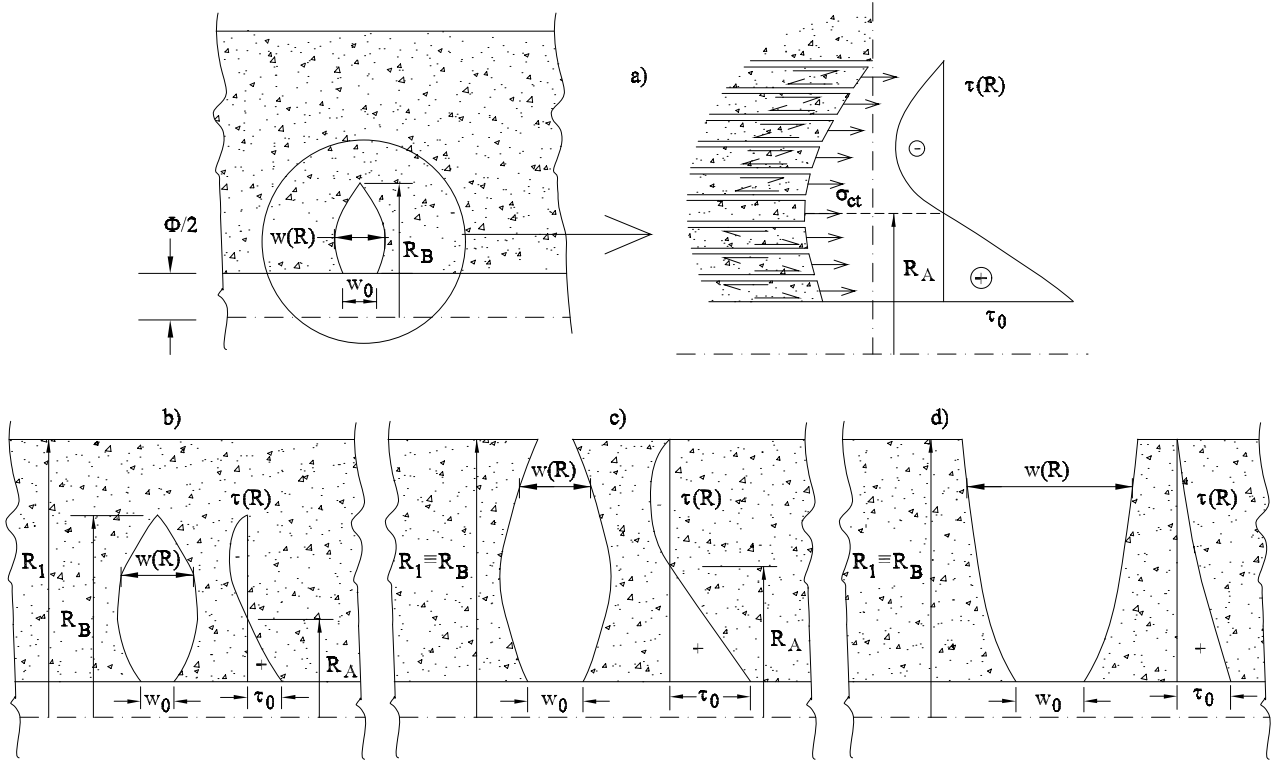


Figure 4: Evolution of crack profile: a) directions of shear stress  $\tau(R)$ ; b) internal crack; c-d) evolution of a main crack.

Such a consideration is confirmed by the tests of Scott & Gill (1987), who have measured the displacement profile of the concrete in one of the ends of a RC tie. In this cross-section, where  $\sigma_{ct}=0$ , they found a displacement field similar to the shape of crack profile  $w(R)$  reported in Figure 4d. Thus, the situation  $R_A=R_1=R_B$  (Fig. 4d) corresponds to the condition  $w_0 \geq w_c$  in the cohesive model of Figure 2c (in which  $w_c$  is the maximum crack width with non-zero stresses). In the other cases (Figs. 4b-4c), a linear variation of  $R_A$ , within the domain  $[\Phi/2, R_1]$ , can be related to the variation of  $w_0$  in the domain  $[0, w_c]$ . In this way,  $R_A$  is given by:

$$R_A = \Phi/2 + (R_1 - \Phi/2) \frac{w_0}{w_c} \quad \text{if } w_0 < w_c \quad (6)$$

$$R_A = R_1 \quad \text{if } w_0 \geq w_c$$

Similarly, the definition of function  $\gamma$  (Eq. [5]) is ruled by the value of  $w_0$ . In particular, when  $w_0 \geq w_c$ ,  $\tau(R)$  is a monotonic function and consequently  $\gamma \geq -1$ . In the case  $w_0 < w_c$ ,  $\tau(R)$  must be equal to zero at the distances  $R_B$  and  $R_A$  from the reinforcement axis (that is,  $\gamma < -1$  in the domain  $[R_A, R_B]$ , and  $\gamma > -1$  in the domain  $[R_0, R_A]$ ). Under these conditions, it is assumed that the function  $\partial\sigma_{ct}/\partial z$  takes the following form:

$$\frac{\partial\sigma_{ct}}{\partial z} = (R_1 - R_A) \cdot (a + b \cdot R) + c \quad \text{if } w_0 < w_c \quad (7)$$

$$\frac{\partial\sigma_{ct}}{\partial z} = c \quad \text{if } w_0 \geq w_c$$

where  $a, b, c =$  coefficients. Substituting Eqs. (6) and Eqs. (7) into Eq. (5), the function  $\gamma(R)$  becomes:

$$\gamma(R) = \frac{1}{\tau_0 \cdot R_0} \left[ \frac{R^2 - R_0^2}{2} c + (R_1 - R_0) \left( 1 - \frac{w_0}{w_c} \right) \cdot \left( \frac{R^2 - R_0^2}{2} a + \frac{R^3 - R_0^3}{3} b \right) \right] \quad \text{if } w_c < w_0 \quad (8)$$

$$\gamma(R) = \frac{1}{\tau_0 \cdot R_0} \cdot \frac{R^2 - R_0^2}{2} c \quad \text{if } w_c \geq w_0$$

For a given value of  $R_B$  ( $\leq R_1$ ), the coefficients  $a, b$  and  $c$  can be evaluated by imposing, simultaneously, the following boundary conditions:

$$w_0 < w_c \Rightarrow \begin{cases} \gamma = -1 & \text{if } R = R_A \\ \gamma = -1 & \text{if } R = R_B \end{cases} \quad (9)$$

$$w_0 \geq w_c \Rightarrow \gamma = -1 \quad \text{if } R = R_B$$

When  $a, b$  and  $c$  are known, both  $\gamma(R)$  and  $\tau(R)$  can be evaluated by means of Eqs. (8) and Eq. (4), respectively.

## 2.2 The radial displacement $v(R)$ function

Due to the longitudinal slip  $s(z)$  between steel and concrete, a radial displacement  $v(R)$  can be also observed around the ribs of deformed bars. The description of the complete steel-concrete interaction, introduced by Tepfers (1979), is schematically reproduced in Figure 5a. More precisely, the slips  $s(z)$  produce crushing of the concrete in front of the ribs. Sliding planes, inclined of  $\beta=30^\circ \div 40^\circ$  with respect to the reinforcement axis, are generated by this phenomenon. The displacement is therefore independent of the rib face angle, when it exceeds  $40^\circ$ .

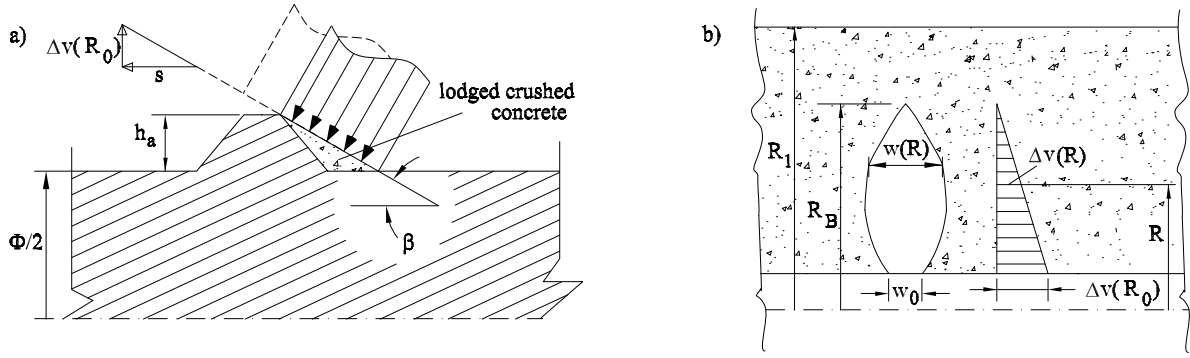


Figure 5: Definition of  $\Delta v(R)$ : a) concrete displacements around the ribs; b) possible distribution of  $\Delta v(R)$  around the cracked cross-section.

The increment of radial displacements  $\Delta v$ , which must be introduced in Eq. (1), is therefore a function of the longitudinal slip  $s(z)$ . Consequently, on the reinforcing bar of the cracked cross-section, where  $s=w_0/2$ , it is possible to obtain  $v(\Phi/2)=\Delta v(\Phi/2)=\tan \beta w_0/2$ . Since the vertical concrete ring in tension (Fig. 2a) resists to the vertical displacement, the condition  $\Delta v(R_B)=0$  is here assumed. On the contrary, in the range  $\Phi/2 \leq R \leq R_B$  (Fig. 5b), the following linear variation of  $\Delta v(R)$  is considered:

$$\Delta v(R) = \frac{w_0}{2} \cdot \tan \beta \cdot \left( 1 - \frac{R - \Phi/2}{R_B - \Phi/2} \right) \leq h_a \quad (10)$$

where  $h_a$  = rib depth of reinforcing bars.

Since ribs on deformed rebars play a fundamental role in the definition of  $\Delta v(R)$  (Eq. [10]), in the present model the shape of the crack profile  $w(R)$  (Eq. [1]) seems to be strictly connected to the type of reinforcement. This is in accordance with the theoretical and experimental observations of Walraven & Reinhardt (1981). In their tests,  $w(R)$  appears nearly constant, independently of the external load  $N$ , if smooth steel reinforcement is adopted.

### 3 A POSSIBLE SOLUTION OF THE PROBLEM

The problem previously formulated can be divided into two parts. In a first step, the crack profile  $w(R)$  can be evaluated from Eq. (1). Afterward, the computed  $w(R)$  can be used in the evaluation of the structural response of cracked RC members in tension. A similar problem has been solved under the hypothesis of parallel crack surfaces [ $w(R)=\text{constant}$ ] (Fantilli et al., 1998; Fantilli et al., 2005). However, both this hypothesis and the assumption of plain and vertical strain profile in each cross-section of a RC tie are here removed.

In the evaluation of  $w(R)$ , instead of  $N$ , the crack width  $w_0$  at steel-concrete interface (Fig. 2d) is considered as the independent variable. This choice depends on the relationship between  $w(R)$  and the applied load  $N$  that can be obtained from a test, during

which the displacements in the end sections of a RC tie are generally controlled. There is not a one-to-one correspondence between  $w(R)$  and  $N$ , because of the softening behavior subsequent to the formation of the main cracks. In other words, crack growth produces a temporary unstable behavior of the member, during which an increase of the average elongation and a reduction of the applied load  $N$  can be measured (Fantilli et al., 1998). Since the width of a single crack increase monotonically (Bosco et al., 1990), for a given  $w_0$ , it is possible to define univocally the crack profile  $w(R)$  and the corresponding applied load  $N$ . To define the crack width  $w$  at a distance  $R$  from the reinforcement axis, all the increments  $\Delta w(R)$ , measured by means of Eq. (1) in the domain  $[\Phi/2, R]$ , must be added to  $w_0$ . If the  $\tau_0-s$  relationship (Fig. 2b) and the mechanical properties of concrete and steel are known, the function  $w(R)$  can be computed by applying an iterative procedure. When  $w(R)$  is known, the state of stress  $\sigma_{ct}(w)$  on the crack surfaces can be defined by the cohesive model  $\sigma_{ct}-w$  of Figure 2c. If  $R_B < R_1$ , in the ligament of internal cracks a uniform stress (equal to the tensile strength  $f_{ct}$ ) is considered. For the evaluation of steel stress in the cracked cross-section  $\sigma_s(z=0)$ , and of the applied load  $N$ , it is necessary to formulate a tension stiffening problem. According to Fantilli et al. (1998), it consists of a system of equilibrium and compatibility equations, as in a classical structural problem.

### 4 ANALYSIS OF R/FRCC AND R/HPFRCC MEMBERS IN TENSION

The Broms' method of measuring crack widths cannot be easily applied to fiber reinforced concrete, because of narrow crack widths. In case of thick concrete covers, it is very difficult, or totally impossible, to measure crack profiles around the steel-concrete surface, even at the failure of the structure. For this reason, to evaluate  $w(R)$  in fiber reinforced concrete structures, a X-ray technique has been adopted by Mihashi et al. (2003).

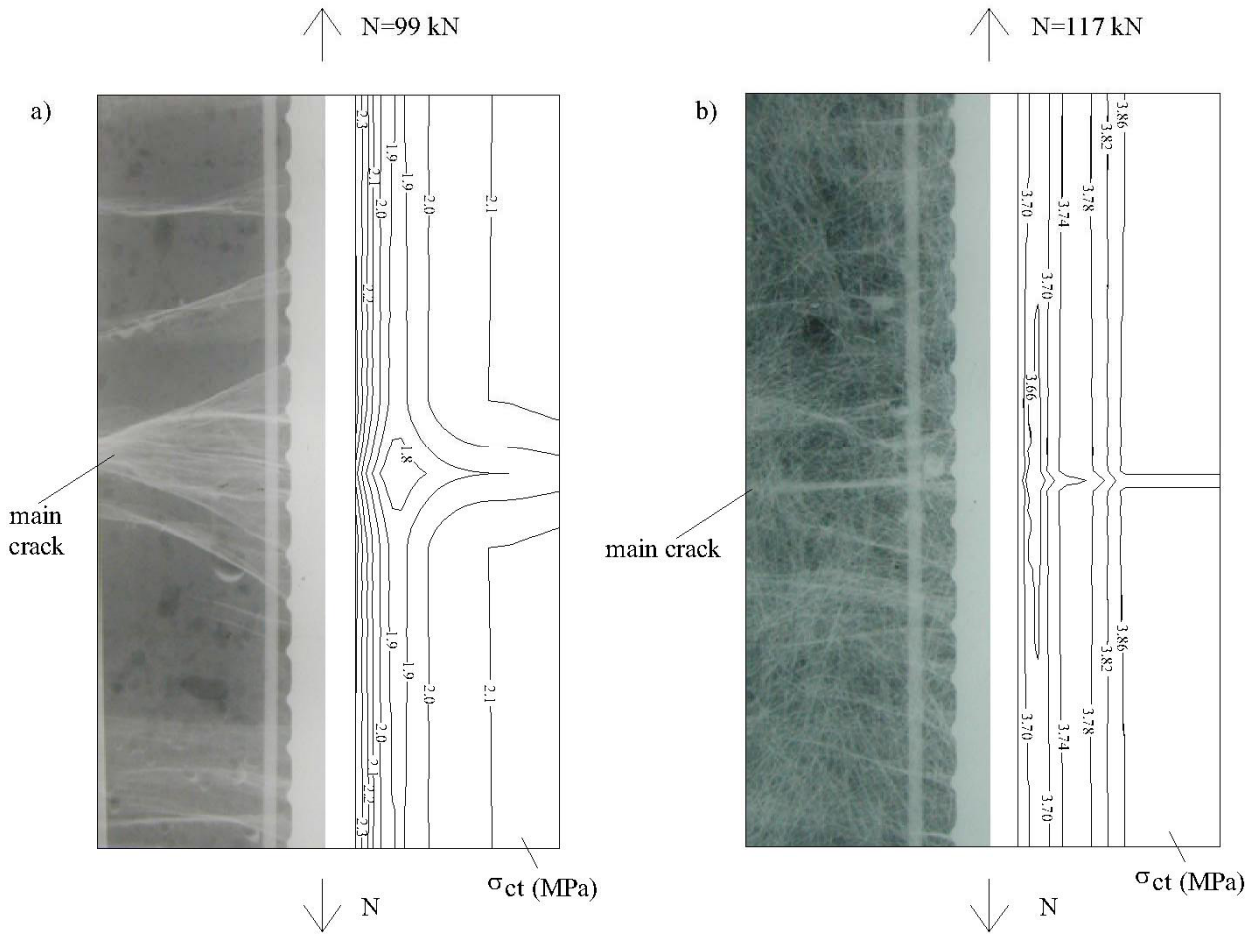


Figure 6: Comparison between the X-ray photographs (Mihashi et al., 2003; Otsuka et al., 2003), and  $\sigma_{ct}$  distributions obtained with the proposed model (contour lines on the right): a) R/FRCC specimen at steel yielding; b) R/HPFRCC specimen at steel yielding.

Two ties tested, named R/FRCC and R/HPFRCC, are here considered. They consist of a single deformed bar of diameter  $\Phi=16$  mm embedded in the center of a rectangle cross-section prism made by FRCC, containing only polyethylene fibers, or by HPFRCC containing steel cords with polyethylene fibers. The geometrical properties of the specimens, the test equipment, and the mechanical properties of the cement-based composites are shown in Mihashi et al. (2003). In these elements, the observation of crack pattern was possible by means of the Otsuka's technique (1989), which consists of injecting a contrast medium into holes embedded in the specimen, and taking radiographs at certain stages of loading. Figure 1c and Figure 1d show the X-ray photographs taken at yielding of rebar ( $\sigma_s=420$  MPa), respectively in the R/FRCC and in the R/HPFRCC ties (Mihashi et al., 2003). In both the specimens, the X-ray photographs seem to show qualitatively the stress distribution in the cement-based composite around the main crack. In fact, where the higher values of  $\sigma_{ct}$  have been reached, there is higher concentration of micro-cracks and, consequently, a greater presence of white parts in the radiographs.

In correspondence of a certain value of  $N$ , a qualitative comparison between the stress distribution in

the cement-based composite around the main crack, obtained from the proposed model, and the X-ray photograph can be shown. This is possible by assuming that the bond-slip relationship and the aggregate interlock mechanism (Fig. 2) can be extended to fiber reinforced composites.

Unfortunately these relationships, regarding FRCC and HPFRCC, are still unknown. However, since the comparison has to be only qualitative, the bond-slip relationship and the Rough Cracks model valid for ordinary concrete are here adopted. At steel yielding, Figure 6 shows the comparison between the  $\sigma_{ct}$  distributions in the two cement-based composites (FRCC in Fig. 6a, and HPFRCC in Fig. 6b) and the X-ray photographs. It is possible to observe a distinct similarity between the shape and the position of the contour lines, which represent the curves at the same tensile stress in the concrete, and the white part of the X-ray images.

Both the X-ray radiographs and the  $\sigma_{ct}$  distributions show the different cracking process in the two specimens. This is due to the different behavior of the cement based composite under tensile actions. In the case of R/FRCC members in tension (Fig. 6a), the decrement of tensile stress affects a wide area of concrete around the main crack. In this zone, the

white parts in the X-ray image also show the localized damage of composite. In this case, the crack is entirely cohesive [ $w(R) < w_c$ ], although the steel reinforcing bar is yielded. As a matter of fact, stresses on the crack surface, and on the surrounding cement-based composite, are different from zero (Fig. 6a). This is also true for R/HPFRCC ties (Fig. 6b), where the reduction of tensile stresses is localized in a restricted area around the main crack. The contour lines do not show a great variation of the tensile stress magnitude, which remains almost equal to the tensile strength of the composite. This is shown by the X-ray photograph of Figure 6b, where the white and the black parts are not clearly separated as in the R/FRCC element (Fig. 6a).

## 5 CONCLUSIONS

A new model, able to define the crack profile in a cementitious composite of reinforced elements in tension, is proposed. The bond-slip mechanism, the fracture mechanics of concrete in tension and the shear resistance of cracked concrete are taken into account. Regarding to fiber reinforced cementitious composites, a good agreement between the distribution of tensile stresses in the composites and the X-ray images is also found in R/FRCC and R/HPFRCC members in tension. In these ties, made of cement-based composites having a higher fracture energy, or a strain hardening, cracks are much narrower than in RC ties. Moreover, crack widths are larger on the interface between steel rebar and concrete than on the surface of concrete cover, even after yielding of the rebar.

## ACKNOWLEDGEMENTS

This work has been financially supported by the Italian Ministry of Education, University and Research (PRIN 2004-2005).

## REFERENCES

- ACI Committee 224, 1986. Cracking of Concrete Members in Direct Tension. *ACI Journal* 83(1): 3-13.
- Bazant, Z. P., & Gambarova, P., 1980. Rough Cracks in Reinforced Concrete. *Journal of Structural Division ASCE* 106(4): 819-842.
- Beeby, A.W. 1972. A study of cracking in reinforced concrete members subjected to pure tension. *Cement and Concrete Association, Technical Report n.42.468*, London, U.K.
- Beeby, A.W., 2004. The influence of the parameter  $\phi/\rho_{\text{eff}}$  on crack widths. *Structural Concrete* 5(2):71-83.
- Bianchini, A. C., Kesler, C.E., and Lott, J.L., 1968. Cracking of Reinforced Concrete Under External Load. In *ACI-SP 20, Causes, mechanism and control of cracking in concrete*: 73-85.
- Bosco, C., Carpinteri, A., and Debernardi, P.G., 1990. Fracture of Reinforced Concrete: Scale Effect and Snap-Back Instability. *Engineering Fracture Mechanics* 35(4/5): 665-677.
- Broms, B.B., 1965. Crack Width and Crack Spacing in Reinforced Concrete Members. *ACI Journal Proceedings*, 62(10): 1237-1256.
- Comité Euro-International du Béton (CEB), 1993. CEB-FIP Model Code 1990. *CEB Bulletin d'Information n. 213/214*, Lausanne, Switzerland.
- Dei Poli, S., Gambarova, P. G., and Karakoc, C., 1986. Aggregate Interlock Role in R.C. Thin-Webbed Beams in Shear. *Journal of Structural Engineering ASCE* 113(1): 1-19.
- Fantilli, A.P., Ferretti, D., Iori, I., and Vallini, P., 1998. Behaviour of R/C elements in bending and tension: the problem of minimum reinforcement ratio. In A. Carpinteri (ed) *Minimum Reinforcement in Concrete Members,ESIS Publication 24*, Elsevier, Amsterdam, The Netherlands: 99-125.
- Fantilli, A.P., Mihashi, H., and Vallini, P., 2005. Strain Compatibility between HPFRCC and Steel Reinforcement. *Materials and Structures* 38(5): 495-503.
- Gambarova, P. G., 1980. On Aggregate Interlock Mechanism in Reinforced Concrete Plates with Extensive Cracking. *Studi e Ricerche, Corso di Perfezionamento per le Costruzioni in Cemento Armato F.lli Pesenti, Politecnico di Milano*, Vol. 2: 43-102 (in Italian).
- Goto, Y., 1971. Crack Formed in Concrete Around Deformed Tension Bars. *ACI Journal Proceedings* 68(4): 244-251.
- Hillerborg, A., Modéer, M., and Petersson, P. E., 1976. Analysis of crack formation and crack growth in concrete by means of fracture mechanics and finite elements. *Cement and Concrete Research* 6(6): 773-782.
- Lutz, L. A., 1970. Analysis of Stresses in Concrete Near a Reinforcing Bar Due to Bond and Transverse Cracking. *ACI Journal Proceedings* 67(10): 778-787.
- Mihashi, H., Kawamata, A., Kiyota, M., Otsuka, K., and Suzuki, S., 2003. Bond Crack and Tension Stiffening Effect in High-Performance Cementitious Composite. In *Japan Concrete Institute JCI Symposium on Ductile Fiber Reinforced Cementitious Composites (DFRCC)*, Tokyo, Japan: 1-8.
- Otsuka, K., 1989. X-ray technique with contrast medium to detect fine cracks in reinforced concrete. In *Mihashi et al. (Eds) Fracture Toughness and Fracture Energy*, Sendai, Japan: 521-534.
- Otsuka, K., Mihashi, H., Kiyota, M., Mori, S., and Kawamata, A., 2003. Observation of multiple cracking in hybrid FRCC at micro and macro levels. *Journal of Advanced Concrete Technology* 1(3): 291-298.
- Scott, R. H., & Gill, P. A. T., 1987. Short-term distributions of strain and bond stress along tension reinforcement. *The Structural Engineer* 65B(2): 39-48.
- Tepfers, R., 1979. Cracking of concrete cover along anchored deformed reinforcing bars. *Magazine of Concrete Research* 31(106): 3-12.
- Walraven, J. C., & Reinhardt, H. W., 1981. Theory and Experiments on the Mechanical Behaviour of Cracks in Plain and Reinforced Concrete Subjected to Shear Loading. *Heron* 26(1A): 1-68.
- Watstein, D., & Mathey, R. G., 1959. Width of Cracks in Concrete at the Surface of Reinforcing Steel Evaluated by Means of Tensile Bond Specimens. *ACI Journal Proceedings* 55(7): 47-56.